

Article

Slip Microrotation Flow of Silver-Sodium Alginate Nanofluid via Mixed Convection in a Porous Medium

Hossam A. Nabwey^{1,2,*} , Ahmed M. Rashad³  and Waqar A. Khan⁴ 

¹ Department of Mathematics, College of Science and Humanities in Al-Kharj, Prince Sattamin Abdulaziz University, Al-Kharj 11942, Saudi Arabia

² Department of Basic Engineering Science, Faculty of Engineering, Menoufia University, Shebin El-Kom 32511, Egypt

³ Department of Mathematics, Faculty of Science, Aswan University, Aswan 81528, Egypt; am_rashad@aswu.edu.eg

⁴ Department of Mechanical Engineering, College of Engineering, Prince Mohammad Bin Fahd University, Al Khobar 31952, Saudi Arabia; wkhan@pmu.edu.sa

* Correspondence: eng_hossam21@yahoo.com or h.mohamed@psau.edu.sa

Abstract: In the previous decennium, considerable applications of nanoparticles have been developed in the area of science. Nanoparticles with micropolar fluid suspended in conventional fluids can increase the heat transfer. Micropolar fluids have attracted much research attention because of their use in industrial processes. Exotic lubricants, liquid crystal solidification, cooling of a metallic plate in a bath, extrusion of metals and polymers, drawing of plastic films, manufacturing of glass and paper sheets, and colloidal suspension solutions are just a few examples. The primary goal of this study was to see how radiation and velocity slip affect the mixed convection of sodium alginate nanofluid flow over a non-isothermal wedge in a saturated porous media. In this communication, the Tiwari and Das model was employed to investigate the micropolar nanofluid flow via mixed convection over a radiated wedge in a saturated porous medium with the velocity slip condition. Nanoparticles of silver (Ag) were used in a sodium alginate base fluid. The intended system of governing equations is converted to a set of ordinary differential equations and then solved applying the finite difference method. Various fluid flows, temperatures, and physical quantities of interest were examined. The effects of radiation on the skin friction are negligible in the case of forced and mixed convection, whereas radiation increases the skin friction in free convection. It is demonstrated that the pressure gradient, solid volume fraction, radiation, and slip parameters enhance the Nusselt number, whereas the micropolar parameter reduces the Nusselt number.

Keywords: mixed convection; micropolar nanofluid; wedge; velocity slip; radiation



Citation: Nabwey, H.A.; Rashad, A.M.; Khan, W.A. Slip Microrotation Flow of Silver-Sodium Alginate Nanofluid via Mixed Convection in a Porous Medium. *Mathematics* **2021**, *9*, 3232. <https://doi.org/10.3390/math9243232>

Academic Editors: Mostafa Safdari Shadloo, Mohammad Mehdi Rashidi and Alessio Alexiadis

Received: 25 November 2021

Accepted: 13 December 2021

Published: 14 December 2021

Publisher's Note: MDPI stays neutral with regard to jurisdictional claims in published maps and institutional affiliations.



Copyright: © 2021 by the authors. Licensee MDPI, Basel, Switzerland. This article is an open access article distributed under the terms and conditions of the Creative Commons Attribution (CC BY) license (<https://creativecommons.org/licenses/by/4.0/>).

1. Introduction

Conventional heat transfer fluids like water and oil are essential because they participate in many industrial operations, and they increase the thermal accessibility of hanging which carries nanoparticles [1]. Although these fluids decrease heat transport capacity, there is a restriction in heat transport operation. There is a way to increase the thermal conductivity by suspending nanoparticles inside the base fluids. The nanofluids introduced by Choi [2] were a mix of nanoparticles, and the base fluid was converted into heat transport fluids with extraordinary higher accessibility. The nanoparticles utilized in the base fluids are prefabricated from metals, non-metals, oxides, or carbides. The shape of nanoparticles may be like disks, rods, spheres, etc. [3], and the base fluids are generally ethylene glycol, water or oil. Several studies have proved that nanofluids have higher thermal conductivities. Recently, a lot of researchers are concerned with the study of nanofluids. Sing et al. [4] explained the action of unsteady mixed convective flow past an orthogonal wedge under the effect of incompressible viscous fluid. Makinde and Aziz [5] investigated the

mixed convective flow of nanofluid through an extension sheet. Patrulescu and Grosan [6] analyzed the boundary layer of mixed convective nanofluids flowing past a vertical cone. Chamkha et al. [7] explained the nanofluid flow by combining convective and radiate wedges. Gorla et al. [8] analyzed the boundary layer of combined convective flow through a wedge-filled nanofluid in porous media. Imtiaz and Hayat [9] investigated a mixed convective flowing for Casson nanofluid past an extension cylinder.

On the other hand, many researchers have shed light on micropolar fluids because of their great importance since they describe the quality of the particles suspended in the fluid successfully. Micropolar fluids are fluids that have the characteristics of fluids with non-symmetric strain tensors. Eringen [10,11] introduced the theory of the micropolar fluid. This theory presents the microscopic effects because of the micromotion and local structure of the fluid elements. The idea of lubrication is an essential application for micropolar fluids. El-Aziz [12] analyzed the unstable combined convective of a micropolar fluid neighboring the hot orthogonal surface since the viscous dispersion exists. Roy and Gorla [13] studied the magnetohydrodynamic mixed convection flow of a micropolar fluid along with an orthogonal wedge. Adnan [14] explained the combined convection past a level plate for a micropolar fluid in a boundary-layer flowing situation. Singh [15] studied the unsteady combined convective flowing of viscous dispersion in a micropolar fluid over a stretching surface under the impact of thermal radiation.

The above literature survey reveals that no effort has been made to explore the impacts of radiation and velocity slip on mixed convection of sodium alginate of micropolar nanofluid flow over a non-isothermal wedge in a saturated porous medium. In this regard, an innovative mathematical formulation is established by using Ag in sodium alginate-based micropolar nanofluid. Moreover, the mixed convection, material, and nanoparticle volume friction phenomena are also measured. Elucidations of micropolar-nanofluid are documented via graphs. This investigation extends earlier explorations and should be helpful for micropolar nanofluid studies.

2. Mathematical Model

Here we concentrate on a 2D steady laminar silver-sodium alginate micropolar nanofluid flow via mixed convection and velocity slip cross a radiative wedge with angle Ω in a porous medium is shown in Figure 1.

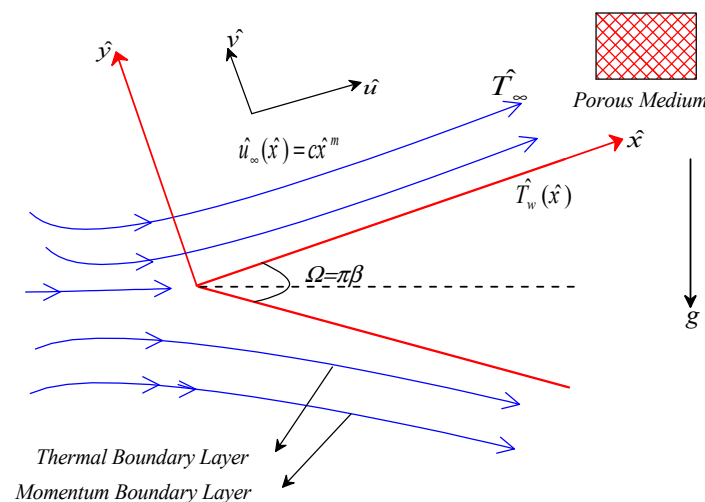


Figure 1. Flow geometry and physical model for radiative wedge.

It is assumed that \hat{x} and \hat{y} are Cartesian coordinates measured along the wedge surface and normal to it, respectively. It is also assumed that the free stream velocity $\hat{u}_\infty(\hat{x}) = c\hat{x}^m$, where a is constant, and m is the Falkner-Skan power-law parameter with $0 \leq m = \beta/(2 - \beta) \leq 1$, since β is Hartree pressure gradient parameter that corresponds to $\beta = \Psi/\Pi$ where Ψ the total wedge angle. It is noted that $\beta = 0$ and $\beta = 1$ correspond

to horizontal and vertical walls cases. The temperature at the wedge surface is believed to be variable $\hat{T}_w(x)$ while the ambient temperature has a constant value \hat{T}_∞ . The flow is considered to be laminar, and a micropolar nanofluid is assumed to be incompressible, uniform properties and thermal equilibrium between the in a sodium alginate-based micropolar nanofluid containing silver (Ag) nanoparticles. The thermophysical properties of the sodium alginate and Ag are listed in Table 1.

Table 1. Thermo-physical properties of base fluid and nanoparticles [16].

Properties	Base Fluid (Sodium Alginate)	Silver (Ag)
Density, ρ (kg/m ³)	989	10,500
Specific heat, c_p (J/kg-K)	4175	235
Thermal conductivity, k (W/m-K)	0.6376	429
Prandtl number, Pr	6.5	-

Using the above hypothesis and the Tiwari and Das model, the simplifying governing equations of the problem can be written as [7,8]:

$$\frac{\partial \hat{u}}{\partial \hat{x}} + \frac{\partial \hat{v}}{\partial \hat{y}} = 0 \tag{1}$$

$$\hat{u} \frac{\partial \hat{u}}{\partial \hat{x}} + \hat{v} \frac{\partial \hat{u}}{\partial \hat{y}} - \hat{u}_\infty \frac{d\hat{u}_\infty}{d\hat{x}} = \frac{\hat{\mu}_{nf} + \hat{\kappa}}{\hat{\rho}_{nf}} \frac{\partial^2 \hat{u}}{\partial \hat{y}^2} + \frac{\hat{\kappa}}{\hat{\rho}_{nf}} \frac{\partial \hat{N}}{\partial \hat{y}} - \frac{\hat{\mu}_{nf} + \hat{\kappa}}{\hat{\rho}_{nf} K_1(\hat{x})} (\hat{u} - \hat{u}_e) + \frac{g(\hat{\rho}\hat{\beta})_{nf}}{\hat{\rho}_{nf}} (\hat{T} - \hat{T}_\infty) \sin \frac{\Omega}{2} \tag{2}$$

$$\hat{u} \frac{\partial \hat{N}}{\partial \hat{x}} + \hat{v} \frac{\partial \hat{N}}{\partial \hat{y}} = \frac{\hat{\gamma}_{nf}}{\hat{\rho}_{nf} J} \frac{\partial^2 \hat{N}}{\partial \hat{y}^2} - \frac{\hat{\kappa}}{\hat{\rho}_{nf} J} (2\hat{N} + \frac{\partial \hat{u}}{\partial \hat{y}}) \tag{3}$$

$$\hat{u} \frac{\partial \hat{T}}{\partial \hat{x}} + \hat{v} \frac{\partial \hat{T}}{\partial \hat{y}} = \hat{\alpha}_{nf} \frac{\partial^2 \hat{T}}{\partial \hat{y}^2} - \frac{1}{(\hat{\rho}c_p)_{nf}} \frac{\partial \hat{q}_r}{\partial \hat{y}} \tag{4}$$

with the boundary conditions:

$$\begin{aligned} \hat{u} &= \hat{A}(\hat{x})\hat{\mu}_{nf} \frac{\partial \hat{u}}{\partial \hat{y}}, \hat{N} = -n \frac{\partial \hat{u}}{\partial \hat{y}}, \hat{v} = 0, \hat{T} = \hat{T}_w(x) \text{ at } \hat{y} = 0 \\ \hat{u} &\rightarrow \hat{u}_\infty(\hat{x}), \hat{T} \rightarrow \hat{T}_\infty, \hat{N} \rightarrow 0 \text{ as } \hat{y} \rightarrow \infty \end{aligned} \tag{5}$$

where \hat{u} is the velocity along the \hat{x} -axis, and \hat{v} is the velocity along the \hat{y} -axis, N is the angular velocity, \hat{T} the temperature of the fluid, g is the acceleration, J is the micro-inertia density, $\hat{\kappa}$ is the vortex viscosity, n is constant since $0 \leq n \leq 1$. If $n = 0$, the concentration becomes strong [17]; if $n = 1/2$, the concentration becomes weak [18], and if $n = 1$, this condition is used in the styling of turbulent boundary-layer flowing [19]. Moreover, the radiative heat flux through the Rosseland approach can be written as:

$$\hat{q}_r = -\frac{4\hat{\sigma}}{3\hat{k}^*} \frac{\partial \hat{T}^4}{\partial \hat{y}}, \tag{6}$$

where \hat{k}^* and $\hat{\sigma}$ are the coefficient of average absorption and the Stefan Boltzmann constant, respectively. It is presumed that the temperature variations induced by the flow are small so that the expression may be considered a linear temperature function. Then, by Taylor's expansion of \hat{T}^4 concerning \hat{T}_∞ and disregarding terms of higher-order, we obtain:

$$\hat{T}^4 \approx -3\hat{T}_\infty^4 + 4\hat{T}_\infty^3 \hat{T} \tag{7}$$

Also, to obtain similarity solutions, we consider the values of the following form:

$$\begin{aligned} \hat{u}_\infty(\hat{x}) &= c\hat{x}^m, \hat{T}_w(\hat{x}) = \hat{T}_\infty + b\hat{x}^{(5m-1)/2}, \hat{K}_1(\hat{x}) = K_1/\hat{x}^{m-1} \\ J(\hat{x}) &= \frac{v_f}{c}\hat{x}^{1-m}, \hat{A}(\hat{x}) = A/\hat{x}^{(m-1)/2} \end{aligned} \tag{8}$$

$$\begin{aligned} \hat{\rho}_{nf} &= (1-\phi)\hat{\rho}_f + \phi\hat{\rho}_s, \hat{\alpha}_{nf} = \frac{\hat{k}_{nf}}{(\hat{\rho}c_p)_{nf}}, (\hat{\rho}c_p)_{nf} = (1-\phi)(\hat{\rho}c_p)_f + \phi(\hat{\rho}c_p)_s \\ \hat{\mu}_{nf} &= \frac{\hat{\mu}_f}{(1-\phi)^{2.5}}, \frac{\hat{k}_{nf}}{\hat{k}_f} = \frac{(\hat{k}_s+2\hat{k}_f)-2\phi(\hat{k}_f-\hat{k}_s)}{(\hat{k}_s+2\hat{k}_f)+\phi(\hat{k}_f-\hat{k}_s)}, \hat{\gamma}_{nf} = (\hat{\mu}_{nf} + \frac{\hat{k}}{2})J(\hat{x}) \\ (\hat{\rho}\hat{\beta})_{nf} &= (1-\phi)(\hat{\rho}\hat{\beta})_f + \phi(\hat{\rho}\hat{\beta})_s \end{aligned} \tag{9}$$

We define the similarity variables for the Equations (1)–(3) as:

$$\begin{aligned} \hat{u} &= c\hat{x}^m F'(\eta), \hat{v} = -\frac{1}{2}\sqrt{cv_f}\hat{x}^{\frac{m-1}{2}}[(m+1)F(\eta) + (m-1)\eta F'(\eta)] \\ \eta &= \hat{y}\sqrt{\frac{c}{v_f}}\hat{x}^{\frac{m-1}{2}}, \hat{N} = c\hat{x}^m\sqrt{\frac{c\hat{x}^{m-1}}{v_f}}G(\eta), \theta(\eta) = \frac{\hat{T}-\hat{T}_\infty}{\hat{T}_w-\hat{T}_\infty}. \end{aligned} \tag{10}$$

In light of Equations (8)–(10), Equations (2)–(5) are transformed into:

$$\begin{aligned} \left(\frac{1}{(1-\phi)^{2.5}} + K\right)F''' - \frac{1}{Da}\left(\frac{1}{(1-\phi)^{2.5}} + K\right)(F' - 1) + \left((1-\phi) + \phi\frac{\hat{\rho}_s}{\hat{\rho}_f}\right)\left(\frac{m+1}{2}FF'' - m(F'^2 - 1)\right) \\ + KG' + \lambda\left((1-\phi) + \phi\frac{(\hat{\rho}\hat{\beta})_s}{(\hat{\rho}\hat{\beta})_f}\right)\theta \sin \frac{\Omega}{2} = 0 \end{aligned} \tag{11}$$

$$\left(\frac{1}{(1-\phi)^{2.5}} + \frac{K}{2}\right)G'' + \left((1-\phi) + \phi\frac{\hat{\rho}_s}{\hat{\rho}_f}\right)\left(\frac{m+1}{2}FG' - \frac{3m-1}{2}F'G\right) - K(2G + F'') = 0, \tag{12}$$

$$\frac{\hat{k}_{nf}}{\hat{k}_f}(1 + Rd)\theta'' + Pr\left((1-\phi) + \phi\frac{(\hat{\rho}c_p)_s}{(\hat{\rho}c_p)_f}\right)\left(\frac{m+1}{2}F\theta' - \frac{5m-1}{2}F'\theta\right) = 0, \tag{13}$$

$$\begin{aligned} F'(0) &= \frac{\delta}{(1-\phi)^{2.5}}F''(0), F(0) = 0, \theta(0) = 1, G(0) = -nF''(0) \\ F'(\infty) &= 0, \theta(\infty) = 0, G(\infty) = 0 \end{aligned} \tag{14}$$

Dimensionless numbers are significant in engineering. They decrease the number of variables representing a system, minimizing the amount of experimental data needed to make scalable system correlations from physical occurrences. Their values depend upon the situation and geometry. These numbers in Equations (11)–(13) are defined as:

$$\begin{aligned} Da &= \frac{K_1c}{v_f}, \delta = A\mu_f\sqrt{\frac{c}{v_f}}, K = \frac{\hat{k}}{\hat{\mu}_f}, \lambda = \frac{Gr_x}{Re_x^{5/2}}, Gr_x = \frac{g\beta_f(\hat{T}_w-\hat{T}_\infty)\hat{x}^3}{v_f^2}, \\ Re_x &= \frac{\hat{x}\hat{u}_\infty(\hat{x})}{v_f}, Rd = \frac{16\hat{\sigma}^*\hat{T}_\infty^3}{3\hat{k}^*\hat{k}_f}, Pr = \frac{(\hat{\rho}c_p)_f}{\hat{k}_f} \end{aligned} \tag{15}$$

The physical quantities of interest are given by:

$$\begin{aligned} C_{fx} &= \frac{1}{\hat{\rho}_{nf}\hat{u}_\infty^2}\left[(\hat{\mu}_{nf} + \hat{k})\frac{\partial\hat{u}}{\partial\hat{y}} + \hat{k}\hat{N}\right]_{\hat{y}=0} \\ Nu_x &= -\frac{\hat{x}\hat{k}_{nf}}{\hat{k}_f(\hat{T}_w-\hat{T}_\infty)}\frac{\partial\hat{T}}{\partial\hat{y}}\Big|_{\hat{y}=0} \end{aligned} \tag{16}$$

In dimensionless form, these quantities can be written as:

$$\begin{aligned} C_{fx}Re_x^{1/2} &= \frac{1}{((1-\phi)+\phi\frac{\hat{\rho}_s}{\hat{\rho}_f})}\left[\frac{1+(1-\phi)^{2.5}(1-n)K}{(1-\phi)^{2.5}}\right]F''(0), \\ Nu_xRe_x^{-1/2} &= -\frac{\hat{k}_{nf}}{\hat{k}_f}\left(1 + \frac{4Rd}{3}\right)\theta'(0). \end{aligned} \tag{17}$$

The thermophysical relations utilized are found in [16].

3. Numerical Technique

The nonlinear ordinary differential Equations (11)–(13) are solved numerically with the boundary conditions (14) using the Keller-box method, which is one of the most important strategies for solving parabolic flow equations, particularly boundary layer equations. These schemes are implicit in second-order precision in both space and time, and they allow for arbitrary step sizes in both time and space (non-uniform). This makes it practical and efficient for solving parabolic partial differential equations. This method is explained by Cebeci and Bradshaw [20,21]. This method consists of the following four significant steps:

- Reduce Equations (11)–(13) and boundary conditions (14) to a first-order system of equations by introducing new dependent variables.
- Write the difference equations using central differences.
- Linearize the resulting algebraic equations by Newton's method and write in a matrix-vector form.
- Use the block-tridiagonal-elimination technique to solve the linear system of equations.

To solve the system of equations, a uniform grid size $\Delta\eta = 0.005$ and tolerance of 10^{-5} are assumed in all simulations. MATLAB 2018a was used for this purpose.

4. Results and Discussion

In this study, mixed convection of micropolar nanofluid flow over a radiative vertical wedge in a saturated porous medium with velocity slip impact is investigated. Numerical simulations are performed for the transformed dimensionless Equations (11)–(13) with boundary conditions (14) using an implicit finite difference method. The thermophysical properties of sodium alginate and Ag nanoparticles are reported in Table 1. The numerical results are validated in Table 2 using available data. The present results are found in good agreement with the existing data.

Table 2. Comparison of skin friction with available data for several values of m when other parameters are absent.

m	Yih [22]	Chamkha et al. [23]	Zaib and Haq [24]	Present Results
0.05	0.21348	0.21380	0.21380	0.21350
0	0.33206	0.33221	0.33260	0.33207
0.333	0.75745	0.75759	0.75740	0.75745
1	1.23259	1.23271	1.23260	1.23259

The impacts of pertinent parameters on the dimensionless velocity of Newtonian and micropolar fluids for a weak concentration ($n = 0.5$) are presented in Figures 2 and 3 in the cases of forced, free and mixed convection. The variation of dimensionless velocity with pressure gradient parameter is depicted in Figure 2a for forced convection, in Figure 2b for mixed convection, and in Figure 2c for free convection. In the case of forced convection, the dimensionless velocity increases, inside the hydrodynamic boundary layer, with an increase in the pressure gradient parameter. The dimensionless velocity converges slowly, and the hydraulic resistance increases with the pressure gradient parameter for the Newtonian fluid ($K = 0$), as shown in Figure 2a. However, due to the higher density of nanoparticles, the micropolar fluid ($K = 2$) generates higher resistance to flow than the Newtonian fluid. The same behavior of the dimensionless velocity can be observed for mixed convection in Figure 2b for both fluids. Due to buoyancy effects, the dimensionless velocity overshoots close to the surface and then attains ambient velocity, as shown in Figure 2c for both fluids. The opposite behavior of the dimensionless velocity can be observed inside the boundary layer. Again, the boundary layer thickness is found to be more significant for micropolar fluids.

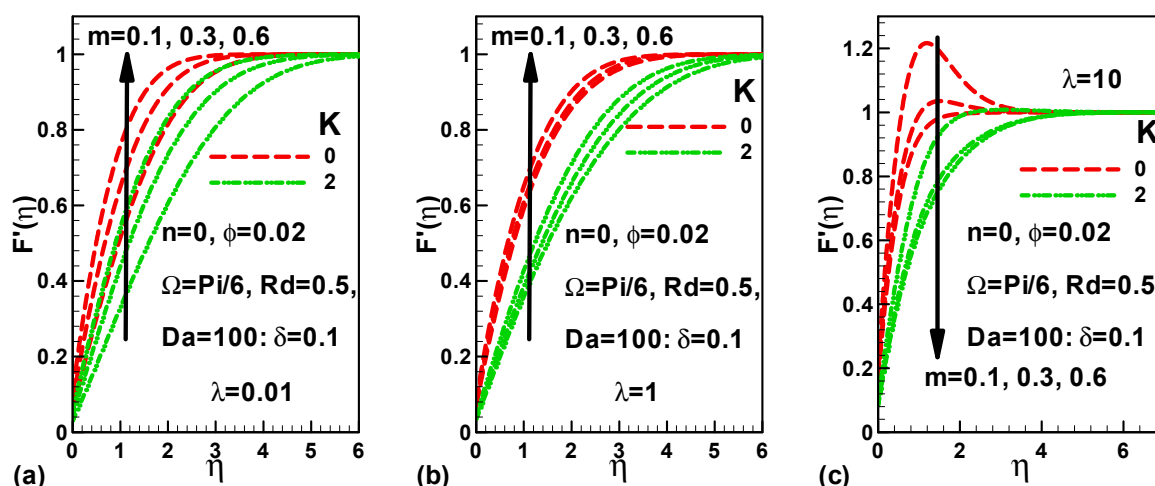


Figure 2. Variation of dimensionless velocity with pressure gradient parameter for (a) forced convection, (b) mixed convection, and (c) free convection.

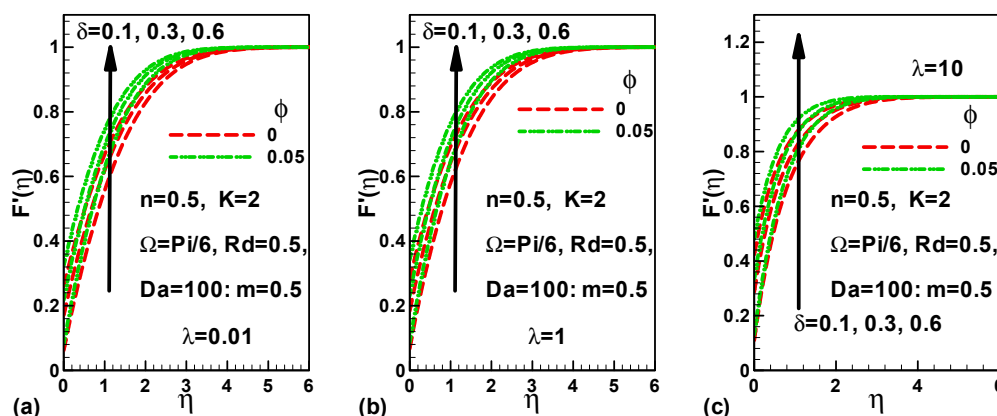


Figure 3. Variation of dimensionless velocity with slip parameter and solid volume fraction of nanoparticles for (a) forced convection, (b) mixed convection, and (c) free convection.

The effects of the velocity slip parameter and solid volume fraction of nanoparticles on dimensionless velocity are demonstrated in Figure 3 for forced, mixed, and free convection. An increase in the slip parameter or solid volume fraction of Ag nanoparticles causes an increase in the dimensionless velocity, which increases the hydrodynamic boundary layer thickness. Thus, the dimensionless velocity increases with both the slip velocity and the solid volume fraction of nanoparticles in each case, as shown in Figure 3a–c. The effects of relevant parameters on the dimensionless temperature are displayed in Figures 4 and 5 for forced, mixed, and free convection, respectively. The dimensionless temperature decreases with an increase in the pressure gradient parameter for both Newtonian and micropolar nanofluid in each case. Consequently, the thermal boundary layer thickness as well as the thermal resistance decrease, as shown in Figure 4a–c. Due to the higher thermal conductivity of the nanoparticles, thermal boundary layers converge quickly for micropolar nanofluid ($K = 2$) in each case. The velocity slip and solid volume fraction of nanoparticles have a negligible effect on the dimensionless temperature for both fluids, as shown in Figure 5a–c for each type of convection heat transfer.

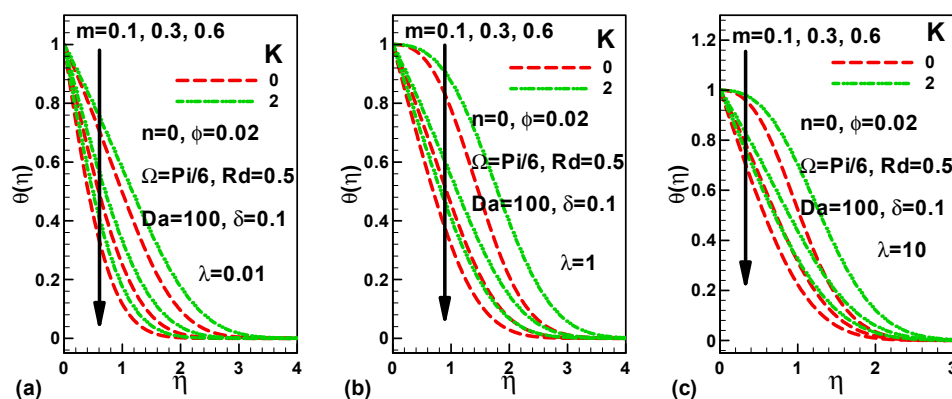


Figure 4. Variation of dimensionless temperature with pressure gradient parameter for (a) forced convection, (b) mixed convection, and (c) free convection.

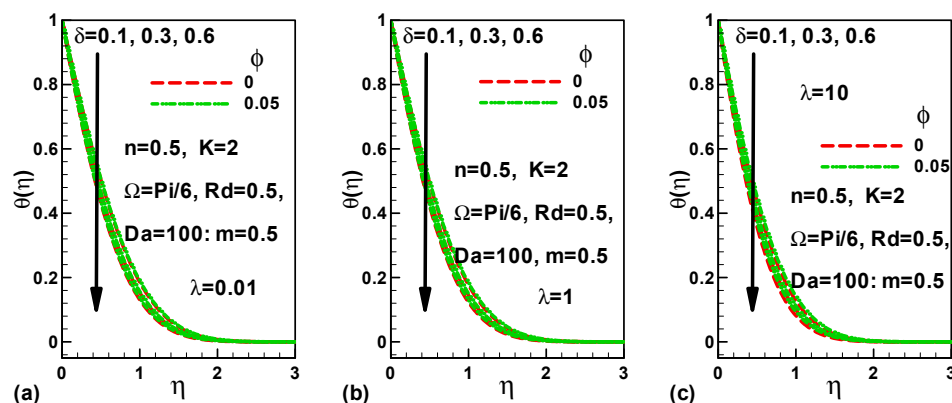


Figure 5. Variation of dimensionless temperature with slip parameter and solid volume fraction of nanoparticles for (a) forced convection, (b) mixed convection, and (c) free convection.

The effects of the pressure gradient parameter on the dimensionless microrotation are displayed in Figure 6a–c for Newtonian and micropolar nanofluid. As expected, for Newtonian fluid, the microrotation velocity is zero in all cases. The microrotation velocity shoots down in the negative direction close to the surface and recovers to satisfy the boundary condition. This happens in each case, and the maximum value of the shooting value depends upon the Richardson number.

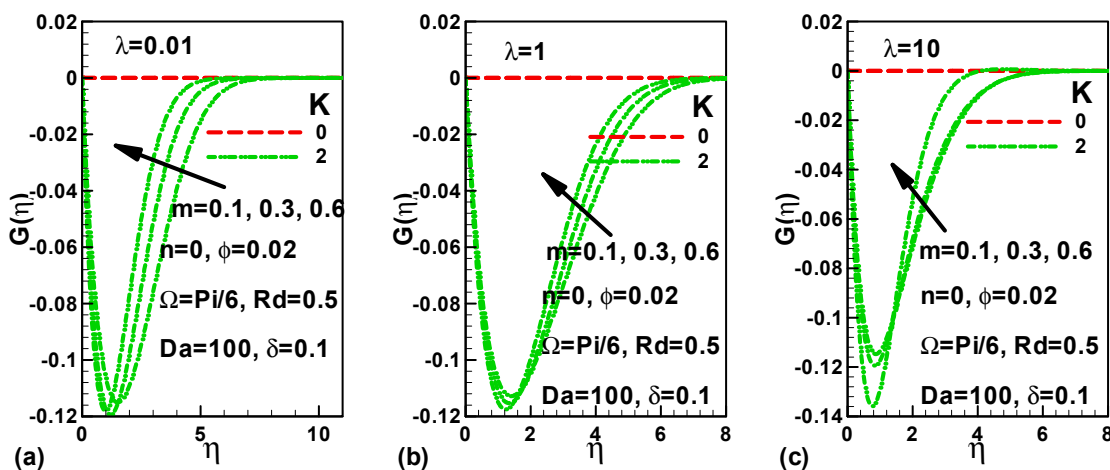


Figure 6. Variation of dimensionless microrotation with pressure gradient parameter for (a) forced convection, (b) mixed convection, and (c) free convection.

The effects of slip velocity and solid volume fraction on the microrotation velocity are illustrated in Figure 7a–c for a micropolar nanofluid with weak concentration. The microrotation velocity is minimum at the surface and increases up to the boundary layer. For the pure micropolar fluid, the microrotation velocity is the least and enhances with the solid volume fraction of nanoparticles. The velocity slip parameter also helps in enhancing the microrotation velocity inside the boundary layer. In free convection, the boundary layer thickness decreases due to the weak concentration of the micropolar nanofluid.

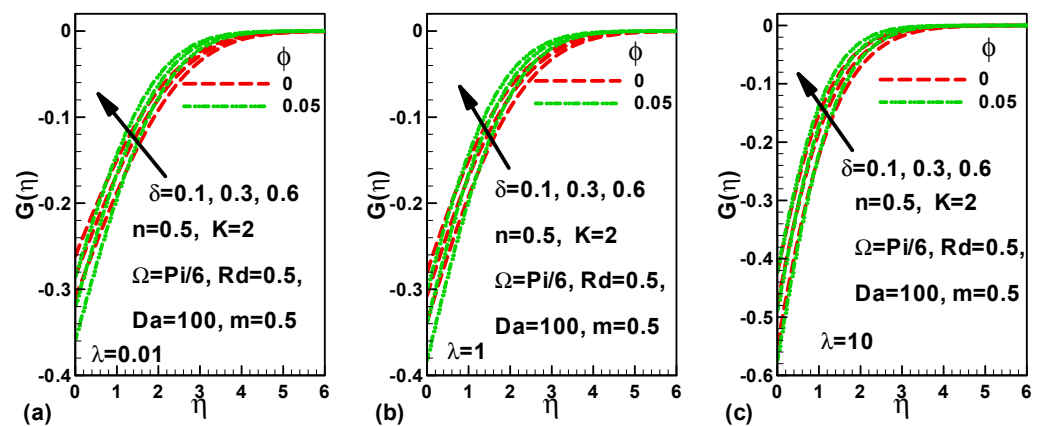


Figure 7. Variation of dimensionless microrotation with slip parameter and solid volume fraction of nanoparticles for (a) forced convection, (b) mixed convection, and (c) free convection.

The variation of skin friction with pertinent parameters is demonstrated in Figures 8 and 9 for Newtonian and micropolar nanofluid with weak concentrations. Figure 8a–c reveal that the skin friction is smaller for Newtonian fluids than micropolar nanofluid. The skin friction increases with the pressure gradient and micropolar parameters. However, the slip velocity parameter helps in reducing skin friction. For the special case of a flat plate ($m = 0$), the skin friction is lowest in the case of forced convection and increases with an increase in the Richardson number. Figure 9a–c depict the variation of skin friction with radiation and solid volume fraction of nanoparticles for different values of Darcy number. It is shown that Darcy number and radiation have no appreciable effect on the skin friction for the forced and mixed convection process (Figure 9a,b). However, in the case of free convection, skin friction increases with the radiation parameter.

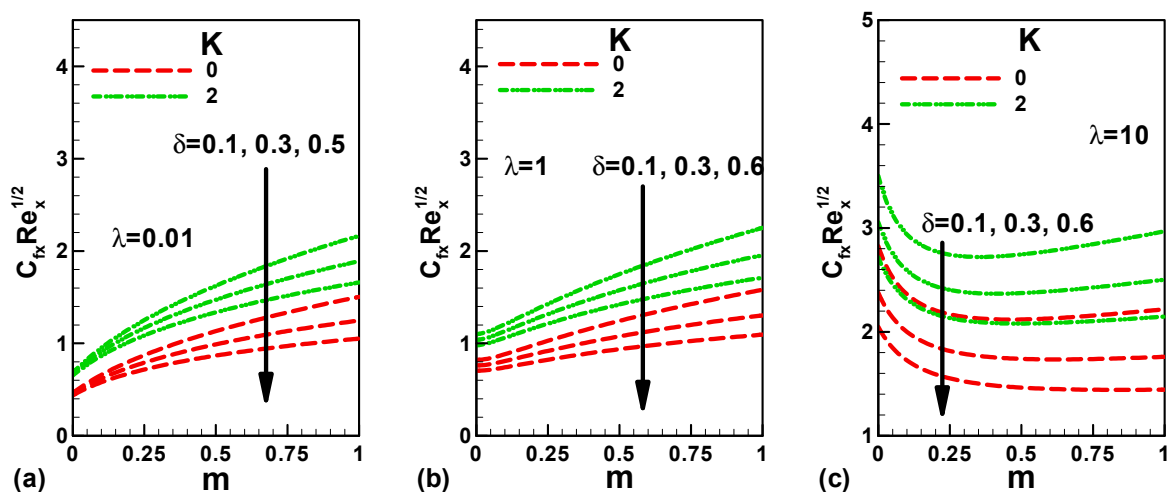


Figure 8. Variation of skin friction with pressure gradient and slip parameters for (a) forced convection, (b) mixed convection, and (c) free convection. [$n = 0.5, \Omega = \pi/6, Rd = 0.5, Da = 100$].

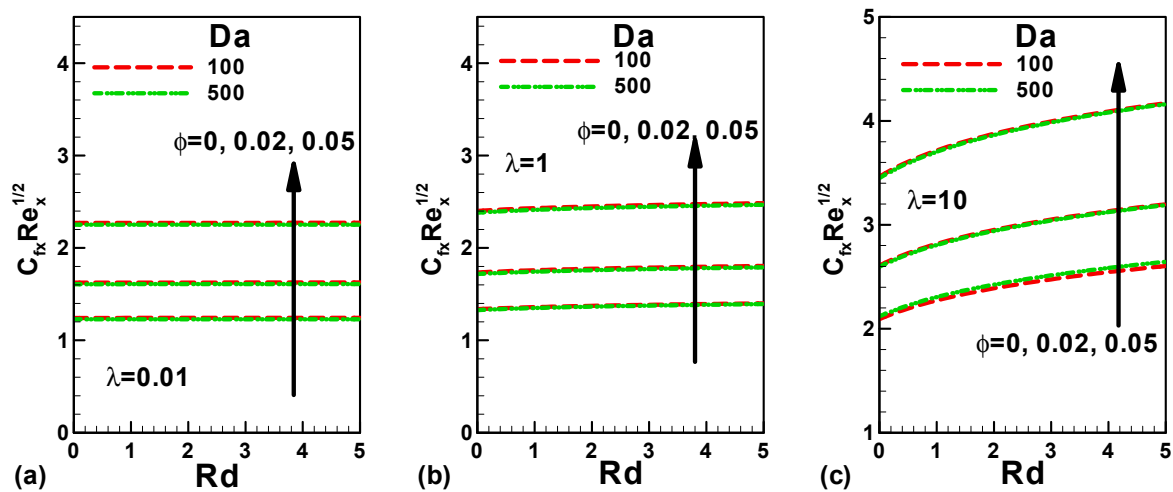


Figure 9. Variation of skin friction with Rd , Da , and ϕ for (a) forced convection, (b) mixed convection, and (c) free convection. [$n = 0.5, \Omega = \pi/6, K = 2, m = 1$].

The variation of Nusselt number with slip and micropolar parameters is shown in Figure 10a for forced convection, in Figure 10b for mixed convection, and in Figure 10c for free convection. The range of Nusselt numbers includes Newtonian to micropolar fluids for two values of pressure gradient parameter. Both velocity slip and pressure gradient parameters help in enhancing the Nusselt number for each fluid. It is important to note that the Nusselt numbers for Newtonian fluids are the highest and decrease with the micropolar parameter. Variation of the Nusselt number with radiation and solid volume fraction of nanoparticles illustrated in Figure 11 for different values of the Darcy number. As expected, the Nusselt numbers increase with both radiation and solid volume fraction of nanoparticles. Due to the higher thermal conductivity of nanoparticles, the dimensionless heat transfer rate increases. Like nanoparticles, radiation also helps in the enhancement of the heat transfer rate of the micropolar nanofluid. The viscous effects increase with an increase in the Darcy number in a porous medium. Consequently, the thermal boundary layer thickness decreases, and the Nusselt number increases.

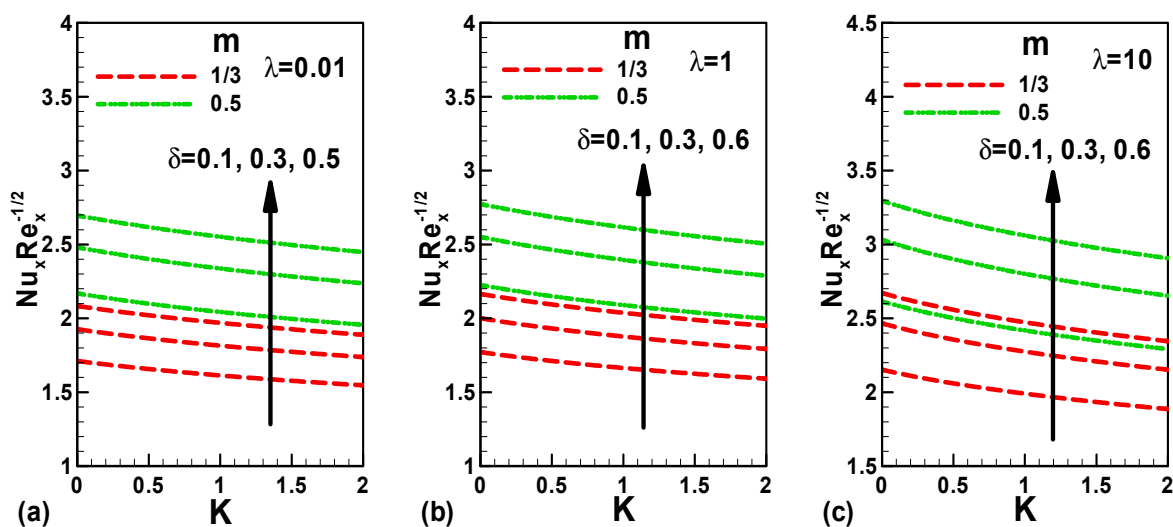


Figure 10. Variation of Nusselt number with pressure gradient and slip parameters for (a) forced convection, (b) mixed convection, and (c) free convection. [$n = 0.5, \Omega = \pi/6, Rd = 0.5, Da = 100$].

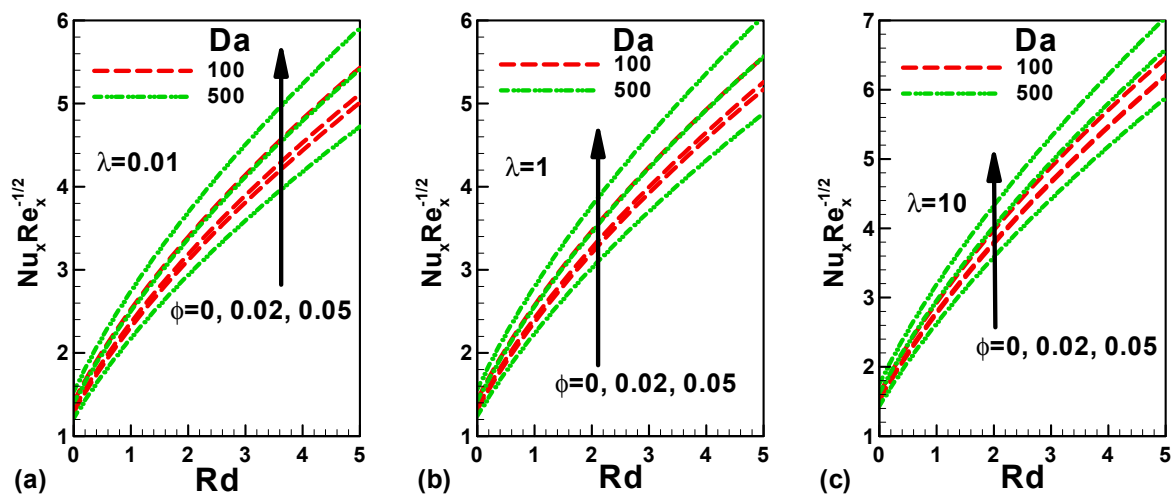


Figure 11. Variation of skin friction with Rd , Da and ϕ for (a) forced convection, (b) mixed convection, and (c) free convection. [$n = 0.5$, $\Omega = \pi/6$, $K = 2$, $m = 1$].

5. Final Conclusions

In this study, mixed convection of micropolar nanofluid is investigated along with a non-isothermal radiative wedge with velocity slip flow. The effects of radiation and other pertinent parameters on the mixed convection of micropolar nanofluid are investigated. The dimensionless governing equations are solved numerically using the Keller-box method. The main conclusions are:

- An increase in the slip parameter or solid volume fraction of Ag nanoparticles causes an increase in the dimensionless velocity.
- The velocity slip and solid volume fraction of nanoparticles have a negligible effect on the dimensionless temperature.
- The dimensionless temperature decreases with an increase in the pressure gradient parameter.
- The velocity slip parameter also helps in enhancing the microrotation velocity inside the boundary layer.
- The skin friction is smaller for Newtonian fluids than micropolar nanofluids.
- The skin friction increases with the pressure gradient and micropolar parameters.
- Darcy number and radiation have no appreciable effect on the skin friction for the forced and mixed convection process.
- Both velocity slip and pressure gradient parameters help in enhancing the Nusselt number for each fluid.
- The Nusselt numbers for Newtonian fluids are highest and decrease with the micropolar parameters.

Author Contributions: Conceptualization, W.A.K.; Methodology, H.A.N., A.M.R. and W.A.K.; Supervision, H.A.N.; Writing—original draft, H.A.N. and A.M.R.; Writing—review—editing, H.A.N., A.M.R. and W.A.K. All authors contributed equally. All authors have read and agreed to the published version of the manuscript.

Funding: The authors extend their appreciation to the Deputyship for Research & Innovation, Ministry of Education in Saudi Arabia for funding this research work through the project number (IF-PSAU-2021/01/17862).

Data Availability Statement: Data available upon request.

Conflicts of Interest: The authors declare no conflict of interest.

Nomenclature

A	Slip factor
C_f	skin friction coefficient
C_p	specific heat at constant pressure
Da	Darcy number
f	stream function
g	acceleration due to gravity
Gr_x	Grashof number
K	micropolar parameter
K_1	permeability of porous medium
k	thermal conductivity
m	Falkner-Skan power-law parameter
Nu	Nusselt number
Pr	Prandtl number
q_r	radiative heat flux
q_w	wall heat flux
Re_x	Reynolds number
Rd	radiation parameter
n, C	constants
\hat{T}_w	wall temperature
\hat{T}_∞	temperature of the ambient nanofluid
\hat{u}, \hat{v}	velocity components along \hat{x} and \hat{y} —directions, respectively
\hat{x} and \hat{y}	are Cartesian coordinates measured along the wedge surface and normal to it
j	microinertia density
N	angular velocity
α	thermal diffusivity
$\hat{\beta}$	thermal expansion coefficient
β	Hartree pressure gradient parameter
ϕ	nanoparticle volume fraction
η	similarity variable
δ	velocity slip parameter
λ	mixed convection parameter
μ	dynamic viscosity
κ	vortex viscosity
ν	kinematic viscosity
θ	dimensionless temperature
ρ	density
τ_w	skin friction or shear stress
ψ	stream function
Ω	angle of the wedge
J	the micro-inertia density
\hat{k}^*	the coefficient of average absorption.
$\hat{\sigma}$	the Stefan Boltzmann constant.
Subscripts	
nf	nanofluid
f	base fluid
s	solid particle
w	wall
∞	infinity

References

- Daungthongsuk, W.; Wongwises, S. A critical review of convective heat transfer of nanofluids. *Renew. Sustain. Energy Rev.* **2007**, *11*, 797–817. [[CrossRef](#)]
- Choi, S.U. Enhancing thermal conductivity of fluids with nanoparticles. *ASME Fluids Eng. Div.* **1995**, *231*, 99–105.
- Rao, Y. Nanofluids: Stability, phase diagram, rheology, and applications. *Particuology* **2010**, *8*, 549–555. [[CrossRef](#)]
- Sing, P.J.; Roy, S.; Ravindran, R. Unsteady mixed convection flow over a vertical wedge. *Int. J. Heat Mass Transf.* **2009**, *52*, 415–421. [[CrossRef](#)]

5. Makinde, O.D.; Aziz, A. Boundary layer flow of a nanofluid past a stretching sheet with a convective boundary condition. *Int. J. Therm. Sci.* **2011**, *50*, 1326–1332. [[CrossRef](#)]
6. Patrulescu, F.-O.; Groşan, T.; Pop, I. Mixed convection boundary layer flow from a vertical truncated cone in a nanofluid. *Int. J. Numer. Methods Heat Fluid Flow* **2014**, *24*, 1175–1190. [[CrossRef](#)]
7. Chamkha, A.J.; Abbasbandy, S.; Rashad, A.M.; Vajravelu, K. Radiation Effects on Mixed Convection over a Wedge Embedded in a Porous Medium Filled with a Nanofluid. *Transp. Porous Media* **2011**, *91*, 261–279. [[CrossRef](#)]
8. Gorla, R.S.R.; Chamkha, A.; Rashad, A.M. Mixed convective boundary layer flow over a vertical wedge embedded in a porous medium saturated with a nanofluid. *Int. Conf. Therm. Issues Emerg. Technol. Theory Appl.* **2010**, *6*, 445–451. [[CrossRef](#)]
9. Imtiaz, M.; Hayat, T.; Alsaedi, A. Mixed Convection Flow of Casson Nanofluid over a Stretching Cylinder with Convective Boundary Conditions. *Adv. Powder Technol.* **2016**, *27*, 2245–2256. [[CrossRef](#)]
10. Eringen, A. Theory of micropolar fluids. *J. Math. Mech.* **1966**, *16*, 1–18. [[CrossRef](#)]
11. Eringen, A. Theory of thermomicrofluids. *J. Math. Anal. Appl.* **1972**, *38*, 480–496. [[CrossRef](#)]
12. El-Aziz, A.M. Mixed convection flow of micropolar fluid from an unsteady stretching surface with viscous dissipation. *J. Egypt. Math. Soc.* **2013**, *21*, 385–394. [[CrossRef](#)]
13. Roy, N.; Gorla, R. Unsteady MHD Mixed Convection Flow of a Micropolar Fluid over a Vertical Wedge. *Int. J. Appl. Mech. Eng.* **2017**, *22*, 363–391. [[CrossRef](#)]
14. Yücel, A. Mixed convection in micropolar fluid flow over a horizontal plate with surface mass transfer. *Int. J. Eng. Sci.* **1989**, *27*, 1593–1602. [[CrossRef](#)]
15. Singh, K.; Kumar, M. Effects of Thermal Radiation on Mixed Convection Flow of a Micropolar Fluid from an Unsteady Stretching Surface with Viscous Dissipation and Heat Generation/Absorption. *Int. J. Chem. Eng.* **2016**, *2016*, 8190234. [[CrossRef](#)]
16. Alwawi, F.A.; Alkawasbeh, H.T.; Rashad, A.M.; Idris, R. MHD Natural Convection of Sodium Alginate Casson Nanofluid over A Solid Sphere. *Results Phys.* **2020**, *16*, 102818. [[CrossRef](#)]
17. Peddieson, J. An application of the micropolar fluid model to the calculation of a turbulent shear flow. *Int. J. Eng. Sci.* **1972**, *10*, 23–32. [[CrossRef](#)]
18. Jena, S.; Mathur, M. Similarity solutions for laminar free convection flow of a thermomicrofluid past a non-isothermal vertical flat plate. *Int. J. Eng. Sci.* **1981**, *19*, 1431–1439. [[CrossRef](#)]
19. Ahmadi, G. Self-similar solution of incompressible micropolar boundary layer flow over a semi-infinite plate. *Int. J. Eng. Sci.* **1976**, *14*, 639–646. [[CrossRef](#)]
20. Cebeci, T.; Bradshaw, P. *Physical and Computational Aspects of Convective Heat Transfer*; Springer: New York, NY, USA, 1988.
21. Cebeci, T.; Bradshaw, P. *Momentum Transfer in Boundary Layers*; Hemisphere Publishing Corporation: New York, NY, USA, 1977.
22. Yih, K.A. MHD forced convection flow adjacent to a non-isothermal wedge. *Int. Commun. Heat Mass Transf.* **1999**, *26*, 819–827. [[CrossRef](#)]
23. Chamkha, A.J.; Mujtaba, M.; Quadri, A. Thermal radiation effects on MHD forced convection flow adjacent to a non-isothermal wedge in the presence of a heat source or sink. *Heat Mass Transf.* **2003**, *39*, 305–312. [[CrossRef](#)]
24. Zaib, A.; Haq, R. Magnetohydrodynamics mixed convective flow driven through a static wedge including TiO₂ nanomaterial with micropolar liquid: Similarity dual solutions via finite difference method. *Proc. Inst. Mech. Eng. Part C J. Mech. Eng. Sci.* **2019**, *233*, 5813–5825. [[CrossRef](#)]